



High-speed slot-die coating of primer layers for Li-ion battery electrodes: model calculations and experimental validation of the extended coating window depending on coating speed, coating gap and viscosity

Sandro Spiegel , Alexander Hoffmann, Julian Klemens, Philip Scharfer, Wilhelm Schabel

Received: 27 July 2023 / Revised: 15 October 2023 / Accepted: 21 October 2023
© The Author(s) 2024

Abstract In the battery industry, very thin primer layers are used to improve electrode adhesion on substrates or act as blocker layers to prevent corrosion in case of aqueous cathodes. For these material configurations, high-speed coating is mandatory to ensure the economic viability of the process. One way to realize high-speed coating is a set-up including a slot die and a vacuum box to stabilize the coating bead. Knowledge and prediction of the coating window of thin wet film thicknesses is crucial to design the production process. Therefore, the influence of coating gap and viscosity of shear-thinning fluids on the coating window is investigated with the help of various model fluids. In addition, a prediction model for the calculation of the coating window for high-speed slot-die coating with vacuum box is developed. This model is shown to be valid for the prediction of the coating window for the investigated material systems and coating gaps over the investigated range of coating speeds up to 500 m min^{-1} . For a material system, which corresponds to a real material system for adhesive primer coatings, it is possible to reach a

target wet film thickness of 20–25 μm . This would correspond to a layer thickness of 0.5 μm for a solid content of 2–2.5 wt%.

Keywords Slot-die coating, Coating window, Extended coating window, Primer layer, Vacuum box, High-speed coating, LIB

Abbreviations

Li	Lithium
LIB	Lithium-ion battery
CMC	Carboxymethyl cellulose
ECW	Extended coating window
VCM	Visco-capillary model

Introduction

For manufacturing electrodes for lithium-ion or post-lithium batteries, it is crucial to ensure sufficient adhesion of the electrode active materials to the current collector metal foil, as well as sufficient electrical and ionic conductivity.^{1–3} In addition, a corrosive reaction between the electrode slurry and aluminum current collector is a challenge during manufacturing of aqueous cathodes.^{4–6} Especially for thick, high-capacity electrodes and electrodes with low binder content, it is a major challenge to achieve sufficient adhesion of the active material to the current collector.^{1,2,7–12} Furthermore, there are materials that promise improved cell performance but have poor adhesion.^{13,14} To improve adhesion of electrodes, multilayer configurations with different layer properties are promising.^{10,15–20} Kumberg et al. and Diehm et al. demonstrated concepts for two-layer electrodes with increased binder content in the lower layer and

Supplementary Information The online version contains supplementary material available at <https://doi.org/10.1007/s11998-023-00877-1>.

S. Spiegel (✉), A. Hoffmann, J. Klemens, P. Scharfer, W. Schabel
Thin Film Technology, Karlsruhe Institute of Technology,
Kaiserstraße 12, 76131 Karlsruhe, Germany
e-mail: sandro.spiegel@kit.edu

S. Spiegel, A. Hoffmann, J. Klemens, P. Scharfer, W. Schabel
Material Research Center for Energy Systems (MZE),
Karlsruhe Institute of Technology, Kaiserstraße 12, 76131
Karlsruhe, Germany

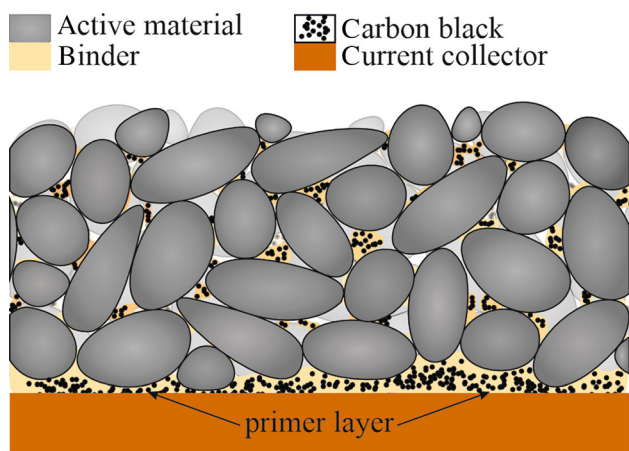


Fig. 1: Schematic representation of the cross section of an electrode consisting of a primer layer (located in the area of the current collector) and an active layer. The primer layer consists of binder and carbon black, and the active layer consists of active material with carbon black and binder

very low binder content in the upper layer of the two-layer electrodes in order to increase adhesion.^{10,17}

Another promising approach to improve adhesion of electrodes is an adhesive primer layer between active material and current collector (see Fig. 1). A primer layer offers the possibility of simultaneously improving adhesion, electrical conductivity and cell performance, even for poorly adhesive electrodes with low binder content. In addition, additive content or binder content in the active layer could be reduced.^{4,21–24} Furthermore, in production of aqueous cathodes, the coating of a primer layer as a blocking layer is an option to prevent corrosion reactions of the active material with the current collector aluminum foil.⁴

Typically, the layer thickness of adhesive primer layers should be in a range of approx. 0.5–2 μm .^{21,24} To inhibit corrosive reactions, the layer thickness of primer layers as blocking layers should be approx. 3–5 μm .⁴ Different layer thicknesses result in different wet film thicknesses, which leads to different settings of the coating gap in production. Diehm et al. used a set-up with slot die and vacuum box, which prevents air-entrainment related defects, allowing to ramp up process speeds with the aim of an economically profitable production of thin aqueous primer layers for graphite anodes with low binder content.²¹ Aqueous processing of primer layers or electrodes reduces production costs, since no solvent recovery has to be taken into account during drying.²⁵ It was also shown that the coated primer layers improve adhesion of the electrode to the current collector without deteriorating cell performance. In addition, process limits were investigated at a constant coating gap. It was shown that an extended coating window (ECW) exists at high coating speeds (approx. $u_w > 100 \text{ m min}^{-1}$) for shear-thinning fluids with the known coating defect mecha-

nism low-flow limit.²¹ In general, the low-flow limit is a common coating defect, occurring as a result of an unstable downstream meniscus and typically visible as stripes in coating direction.^{26–30} For lower coating speeds (approx. $u_w < 100 \text{ m min}^{-1}$), the minimum wet film thickness increases with coating speed, which is well known in the literature. In contrast, for higher coating speeds (approx. $u_w > 100 \text{ m min}^{-1}$), the downstream meniscus is stabilized due to the increasing ratio of inertia to capillary forces and viscous forces. Consequently, the minimum wet film thickness h_{wet} in the extended coating window is significantly lower than conventional predictions by calculations of the low-flow limit. As known from the literature, the low-flow limit is independent from material properties in the dimensionless representation of the coating window.^{21,26} This behavior could not be shown for the extended coating window.^{21,26} Diehm et al. were able to predict the minimum wet film thickness in the extended coating window for high-speed slot-die coating with vacuum box of shear-thinning primer fluids with a defined proportionality factor ($h_{min} = \kappa_{ecw} u_w^{-1/2}$) for a constant coating gap.²¹ Carvalho and Khesghi have also shown the reciprocal proportionality between wet film thickness and coating speed in the extended coating window for different Newtonian fluids ($h_{min} \sim u_w^{-1/2}$) for a constant coating gap.²⁶ In order to optimize formulations or solid content of primer slurries and to be able to adjust the thickness of primer layers and the coating gap as needed, it is important to generate an advanced understanding of high-speed slot-die coating with vacuum box. In the literature, no analytical predictive model for high-speed slot-die coating with vacuum box that includes shear-thinning viscosity and coating gap could be found. Therefore, the influence of different coating gap settings and different viscosities is investigated in this work. To predict the coating window of high-speed slot-die coating with vacuum box as a function of viscosity and coating gap, a combined analytical model, which includes the low-flow limit and the extended coating window, is presented.

Methods

For high-speed slot-die coating with vacuum box, there is a transition area between the common low-flow limit and the extended coating window, in which the inertia effects occurring at higher coating speeds exceed the capillary and viscous forces.^{21,26} In order to predict the operating limits in slot-die coating, the models of the low-flow limit as well as the extended coating window must be combined to cover the entire range of coating speed.

The calculation of the low-flow limit with the visco-capillary model (VCM) is well discussed in the literature [equation (1)].^{26,28,29,31}

$$Ca_{crit} = 0.65 \left[\frac{2}{G^* - 1} \right]^{\frac{3}{2}} \quad (1)$$

In equation (1), capillary number Ca and dimensional coating gap G^* are included. In case of shear-thinning fluids and an approximated Couette flow, the capillary number is defined as [equation (2)]:

$$Ca = \kappa \frac{u_w^n}{\sigma h_G^{n-1}} \quad (2)$$

Including coating speed u_w , coating gap h_G , surface tension σ and the power-law parameters consistency index κ and flow index n . The dimensionless coating gap is the ratio of coating gap h_G to wet film thickness h_{wet} [equation (3)].

$$G^* = \frac{h_G}{h_{wet}} \quad (3)$$

The minimum wet film thickness for the low-flow limit $h_{min, low flow}$ of shear-thinning fluids can be derived from equations (1)–(3).^{30,32}

$$h_{min, low flow} = h_G \left[2 \left(\frac{\kappa u_w^n}{0.65 \sigma h_G^{n-1}} \right)^{-\frac{2}{3}} + 1 \right]^{-1} \quad (4)$$

In addition, the maximum dimensionless coating gap for the low-flow limit $G_{max, low flow}^*$ can be calculated using equations (1) and (2).

$$G_{max, low flow}^* = 2 \left(\frac{\kappa u_w^n}{0.65 \sigma h_G^{n-1}} \right)^{-\frac{2}{3}} + 1 \quad (5)$$

To predict the extended coating window, the boundary-layer theory of Sakiadis has to be taken into account. The boundary-layer theory is based on the Navier–Stokes equation balancing viscous force and inertial force and neglecting gravity and pressure gradient. The theory states that a displacement thickness, which is accelerated by a solid surface, depends on the growth of a viscous boundary layer in y -direction (see Fig. 2).³³ In Fig. 2, the transfer of boundary-layer theory to slot-die coating is shown. p_{vac} is the vacuum pressure adjustable by the vacuum box, p_{atm} is the ambient pressure and Re is the Reynolds number.

In pre-metered coating at moderate coating speeds, the displacement thickness h can be numerically calculated from the superimposed velocity field u (pressure driven Hagen–Poiseuille flow and Couette flow) for a liquid entrainment accelerated by a solid surface or substrate moving with velocity u_w [equation (6)].^{33,34} In this case, inertia forces are low (low Reynolds numbers Re and low Weber numbers We).

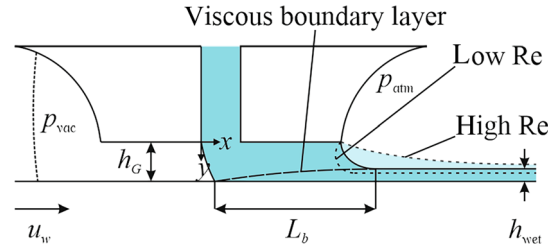


Fig. 2: Schematic illustration of the coating bead and the length of the viscous boundary layer L_b

$$h = h_{wet} = \frac{1}{u_w} \int_0^{h_G} u dy \quad (6)$$

At very high coating speeds, flow conditions in the coating bead of pre-metered coating devices are different and the boundary-layer theory has to be taken into account. Hens and Boiy validated the boundary-layer theory for pre-metered coating devices for high Weber numbers We [equation (7)] when inertia forces are high, with ρ being the fluid density.³⁴

$$We = \frac{\rho u_w^2 h_{wet}}{\sigma} \quad (7)$$

Kistler and Schweizer explained that the ratio of length of the viscous boundary layer L_b to wet film thickness h_{wet} is a function of the ratio of inertia and viscous force [equation (8)].²⁷ Due to the conservation of mass, this must be also valid for the ratio of critical length of the boundary layer L_b^* to the minimum wet film thickness h_{min} .²⁶

$$\frac{L_b}{h_{wet}} = \frac{\text{inertia}}{\text{viscous force}} = \frac{L_b^*}{h_{min}} \quad (8)$$

With:²⁷

$$\text{Inertia} = F_i = \rho u_w^2 h_{wet} \quad (9)$$

$$\text{Viscous force} = F_v = \eta u_w \quad (10)$$

In boundary-layer theory, the calculation of the displacement thickness h is numerically derived from the Navier–Stokes equation.³³

$$h = h_{wet} = \underbrace{1.616}_k \left[\frac{L_b \eta}{\rho u_w} \right]^{\frac{1}{2}} \quad (11)$$

According to Hens and Boiy, the displacement thickness h in the boundary-layer theory corresponds to the wet film thickness h_{wet} in pre-metered coating, with η being the viscosity of Newtonian fluids.³⁴ By

rearranging equation (11), the length of the boundary layer L_b can be described as follows [equation (12)]:

$$L_b = \underbrace{0.383}_{1/k^2} \frac{\rho u_w h_{\text{wet}}^2}{\eta} \quad (12)$$

From the literature, equations (11) and (12) are used to build the model presented in this manuscript. Hens and Boiy validated $1/k^2$ for pre-metered coating devices with sufficient accuracy for Newtonian fluids. Therefore, they observed the coating bead of a pre-metered coating device by using an argon laser beam and compared the observed length of the boundary layer to the calculated length of the boundary layer.³⁴ Arzate and Tanguy could also present an adequate accuracy comparing observed and calculated length of the boundary layer for high-speed jet-coating applications for Newtonian and shear-thinning fluids. They observed the impingement region between jet coater and substrate with a video camera. To calculate the viscosity of the shear-thinning fluid, they used a power-law approach and approximated the given viscosity for a corresponding shear rate, determined from the volumetric flow rate.³⁵

Carvalho and Kheshgi rearranged equation (11) derived from boundary-layer theory for prediction of the minimum wet film thickness h_{min} of the extended coating window for high-speed slot-die coating with vacuum box of Newtonian fluids [equation (13)].²⁶

$$h_{\text{min}} > k \left[\frac{L_b^* \eta}{\rho u_w} \right]^{\frac{1}{2}} \quad (13)$$

Without experimentally observing, simulating or calculating the critical length of the boundary layer, a calculation of the minimum wet film thickness is impossible.

According to the boundary-layer theory of Sakiadis, the length of the boundary layer depends on the viscosity of the fluid. Therefore, it is crucial to approximate the unknown critical length of the boundary layer, to predict the minimum wet film thickness in the extended coating window for different shear thinning fluids. The length of the boundary layer for slot-die coating with vacuum box depends on the vacuum pressure and viscosity. Hence, the length of the boundary layer must be dependent on the coating gap for shear-thinning fluids.^{26,34} Due to the complexity of the flow in the coating gap, it is impossible to analytically calculate the viscosity as a function of the shear rate for a given coating gap without numerical methods. Therefore, we neglect the pressure-driven flow component due to high coating speeds and assume a Couette flow in the coating gap at the inner edge of the downstream lip to calculate an effective viscosity as a function of the shear rate η_{calc} . The effective viscosity of shear-thinning fluids in the coating gap is calculated

with experimentally determined consistency factor κ and flow index n .

$$\eta_{\text{calc}} = \kappa \frac{u_w^{n-1}}{h_G^{n-1}} \quad (14)$$

Consequently, the extended coating window prediction model for high-speed slot-die coating with vacuum box for shear-thinning fluids [equation (15)] consists of equations (13) and (14). $L_{b,\text{calc}}^*$ is the calculated critical length of the boundary layer.

$$h_{\text{min}} > k \left[\frac{L_{b,\text{calc}}^* \eta_{\text{calc}}}{\rho u_w} \right]^{\frac{1}{2}} \quad (15)$$

Equation (15) can be rearranged to obtain the dimensionless form of the extended coating window.

$$G^* < \frac{h_G}{k} \left[\frac{L_{b,\text{calc}}^* \eta_{\text{calc}}}{\rho u_w} \right]^{-\frac{1}{2}} \quad (16)$$

Since the critical length of the boundary layer L_b^* and the minimum wet film thickness h_{min} are both unknown, an empirical equation of the form $f(h_G, \eta_w, \rho)$ for $L_{b,\text{calc}}^*$ is determined [equation (17)].

$$L_{b,\text{calc}}^* = a \frac{\rho^b u_w^c h_G^e}{\eta_{\text{calc}}^d} \quad (17)$$

To examine factor a and exponents b , c , d and e of equation (17), the critical length of the boundary layer $L_{b,\text{exp}}^*$ is calculated from the data of the minimum wet film thickness $h_{\text{min,exp}}$ determined in the experiments [equation (18)].

$$L_{b,\text{exp}}^* = \underbrace{0.383}_{1/k^2} \frac{\rho u_w h_{\text{min,exp}}^2}{\eta_{\text{calc}}} \quad (18)$$

The empirical correlation of equation (17) is fitted to the experimentally calculated values of equation (18) using the least squares method. The determined factors and exponents of equation (17) are shown in Table 1.

Table 1: Calculated factors and exponents of equation (17)

Parameter	Value/–
a	0.018
b	1.000
c	0.553
d	0.312
e	1.565

Table 2: CMC content of the used model fluids

CMC-solution	CMC-content/wt%
CMC-A	1.2
CMC-B	0.5
CMC-C	0.3

The coefficient of determination R^2 for $L_{b,exp}^*$ and $L_{b,calc}^*$ is 0.939, which is sufficiently accurate (see Fig. 8). With equations (17) and (18) and the determined factors and exponents, the extended coating window of high-speed slot-die coating with vacuum box can be theoretically predicted for different coating gaps and different viscosities.

Experimental methods and materials

Slurry preparation

Three aqueous solutions with a defined content of carboxymethylcellulose (Sunrose CMC MAC500LC, Nippon Paper Industries) and 0.5 wt% disodium 4,4'-bis(2-sulfonatostyryl)biphenyl (DSBB, TCI Chemicals) were prepared for the investigations (see Table 2).

At first, DSBB was diluted in deionized water for 10 min at 500 rpm using a lab stirrer. Then, for each solution, the corresponding content of CMC was stirred with the water-DSBB-solution for one hour at 500 rpm until CMC was completely diluted. Thereafter, the viscosity of the different solutions was measured with a rotational rheometer using a cone-plate-system (Physika MCR 101, Anton Paar). The cone measuring head had a diameter of 40 mm and a 0.3° angle (CP40-0.3-SN37598). The measuring head was placed with a measuring gap of 0.025 mm ahead of a counter plate with a 60 mm diameter. Shear rate was varied from 1 to 60000 s⁻¹.

Experimental coating set-up and coating window characterization

To investigate the coating windows for high-speed slot-die coating with vacuum box, it is crucial to examine the coating step independently from the drying step. The experiments were carried out on a Development Coater (TSE Troller AG) with a high-precision steel roller (diameter of 300 mm). The concentricity inaccuracy of the roller is < 1 μm. A slot die with vacuum box was mounted with a 30° angle to the center of the roller. The coating set-up with vacuum box and the film characterization methods are shown schematically in Fig. 3.

The Development Coater offers the possibility to adjust precise coating gaps h_G via PET shims (105 μm, 180 μm and 250 μm) between slot die and steel roller.

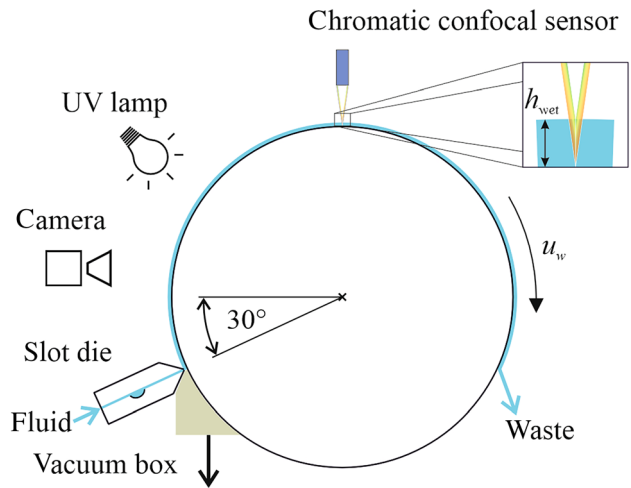


Fig. 3: Schematic figure of the coating set-up with slot die, vacuum box, fluid visualization and film characterization methods

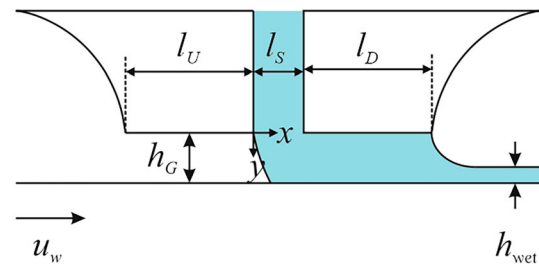


Fig. 4: Schematic figure of the slot die including the length of the upstream and downstream lips $l_U = l_D = 0.5$ mm

The slot width of the slot die was adjusted to $l_S = 200$ μm, and the die outlet width was set to $b_{width} = 150$ mm using a spacer shim. The dimensions of the slot die are shown in Fig. 4.

In the experimental study, coating speeds between 50 and 500 m min⁻¹ were investigated. In all experiments, the vacuum pressure was adjusted until the mechanism of coating defects changed from air entrainment to low-flow limit. Then, the volume flow and, thus, the wet film thickness was adjusted using a pressure tank with a precision needle valve until the coating was stable. To make the defects clearly visible, the UV marker DSBB was used. This procedure was repeated for each coating speed. The pressure tank and the whole fluid handling system is designed for 6 bar maximum feed pressure. The wet film thickness was measured by using a chromatic confocal sensor with measuring range of 600 μm and a resolution of 20 nm in y-direction (CHRcodile SE, Precitec KG).

An image of each of the coating defect was taken and documented to characterize the coating. The following coating defects were observed during the experiments (see Fig. 5). The examples of these coating defects were observed during the investigation of the coating window of CMC-A. The defects have always looked identical for the respective defect mechanisms.

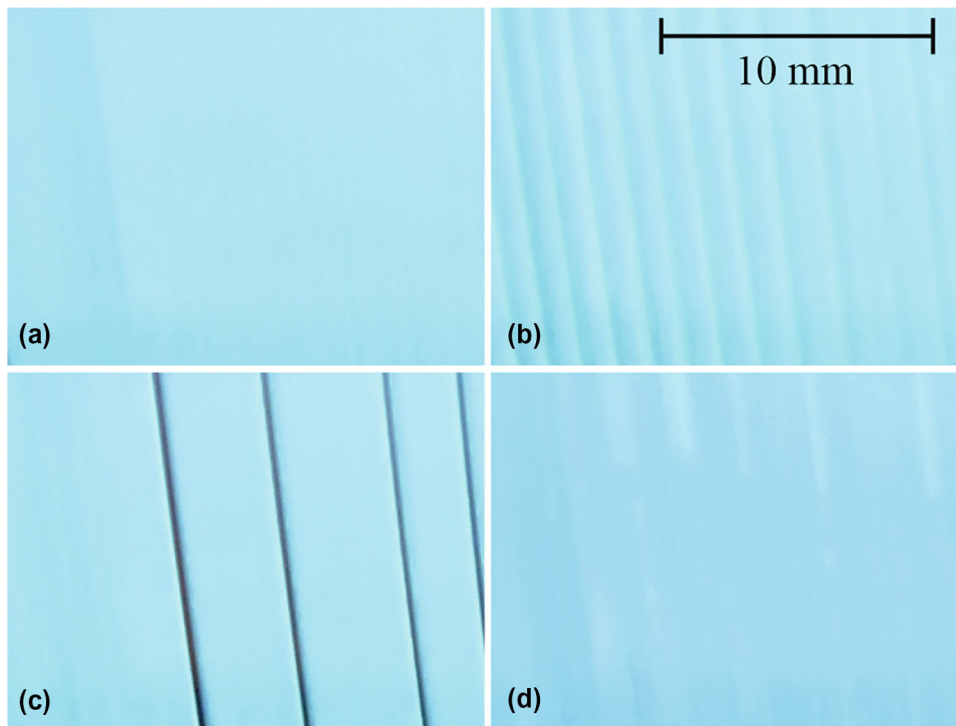


Fig. 5: Top view of a defect-free coating (a) at $u_w = 550 \text{ m min}^{-1}$ and $h_G = 105 \text{ }\mu\text{m}$ with vacuum, low-flow limit (b) at $u_w = 100 \text{ m min}^{-1}$ and $h_G = 250 \text{ }\mu\text{m}$ with vacuum and low-flow limit (c) at $u_w = 100 \text{ m min}^{-1}$ and $h_G = 105 \text{ }\mu\text{m}$ with vacuum and air entrainment (d) at $u_w = 50 \text{ m min}^{-1}$ and $h_G = 250 \text{ }\mu\text{m}$ without vacuum

Results and discussion

Prediction of process stability

To validate the extended coating window prediction model [equations (15) and (17)], different CMC-water solutions with sufficiently large difference in viscosity were used. The viscosity as a function of shear rate of the different material systems is shown in Fig. 6. The minimum and maximum values of the investigated range of shear rate are plotted as vertical black dashed lines (see Table 4).

All model systems show a shear-thinning behavior with different values for consistency factors and flow indices (see Table 3). The viscosity as a function of shear rate decreases from solution CMC-A to CMC-C. To calculate the viscosity for particular model systems, each power-law approach [equation (14)] is valid in the investigated range of shear rate, resulting from the coating gap and the lowest and highest coating speed (see Table 4). The coefficient of determination R^2 is above 0.999 for all calculations in the relevant range of shear rate.

Each model system had a surface tension of approx. 68.57 mN m^{-1} (standard deviation 0.73 mN m^{-1}) and a density of approx. 1017 kg m^{-3} .

In Fig. 7, the prediction of the coating window calculated with the combined model for the low-flow limit (VCM) and the extended coating window (ECW) over the entire range of the investigated process

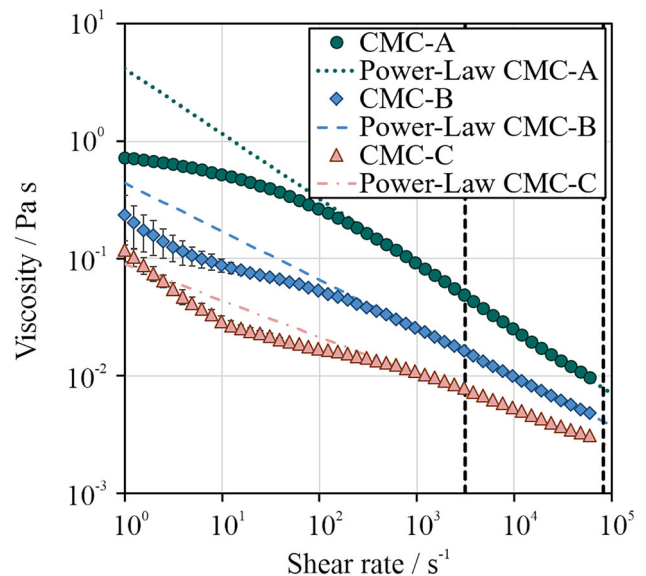


Fig. 6: Measured viscosity (CMC-A dark green circle, CMC-B medium blue diamond, CMC-C light red triangle) and calculated viscosity with power-law approach (CMC-A dark green dotted line, CMC-B medium blue dashed line, CMC-C light red dash-dot line) as a function of shear rate for the different material systems used

parameters and different material systems is shown in dimensionless (left) and exemplarily for one material system in dimensional form (right).

The prediction model shows the expectation of the influence of coating gap and material properties on the low-flow limit and the extended coating window. In the case of the dimensionless coating window (Fig. 7, left), the area for stable coatings in the VCM is below the calculated low-flow limit (purple line). Above the calculated low-flow limit (purple line) coating defects occur, such as stripes in the coating direction.^{26,28} The area for stable coatings in the extended coating window is above the calculated lines of the extended

Table 3: Power-law parameters of the investigated material systems

CMC-solution	$\kappa/\text{Pa s}^n$	$n/-$
CMC-A	4.15	0.45
CMC-B	0.44	0.59
CMC-C	0.09	0.69

Table 4: Ranges of shear rate of the investigated coating gaps and coating speeds

$h_G/\mu\text{m}$	$\dot{\gamma}_{\text{min}}/\text{s}^{-1}$	$\dot{\gamma}_{\text{max}}/\text{s}^{-1}$
105	7936.5	79365.1
180	4629.6	46296.3
250	3333.3	33333.3

coating window in the dimensionless coating window. Below these calculated lines is the unstable area in the extended coating window. As known from literature, the dimensionless low-flow limit line is not affected by material properties. In contrast to the dimensionless low-flow limit, the influence of coating gap and material properties can be seen in the calculation of the dimensionless extended coating window. A decreasing coating gap results in smaller capillary numbers and smaller dimensionless coating gaps [equations (2) and (16)]. For shear-thinning fluids, the coating gap directly influences viscosity. A decreasing viscosity from material system CMC-A to CMC-C leads to a shift of the coating window towards smaller capillary numbers and higher dimensionless coating gaps [equations (2) and (16)]. In addition, a decreasing viscosity reduces the influence of the coating gap on the extended coating window. As a result, the calculated lines for different coating gaps converge with decreasing viscosity.

In the case of the dimensional coating window (Fig. 7, right), the area for stable coatings in the extended coating window is above the calculated lines of the extended coating window. Below these calculated lines is the unstable area in the extended coating window. The area for stable coatings in the VCM is below the calculated low-flow-limit (purple line), and the area for unstable coatings is above the calculated low-flow limit. With increasing coating speed, the minimum wet film thickness increases as explained by the low-flow-limit theory. With increasing stabilization

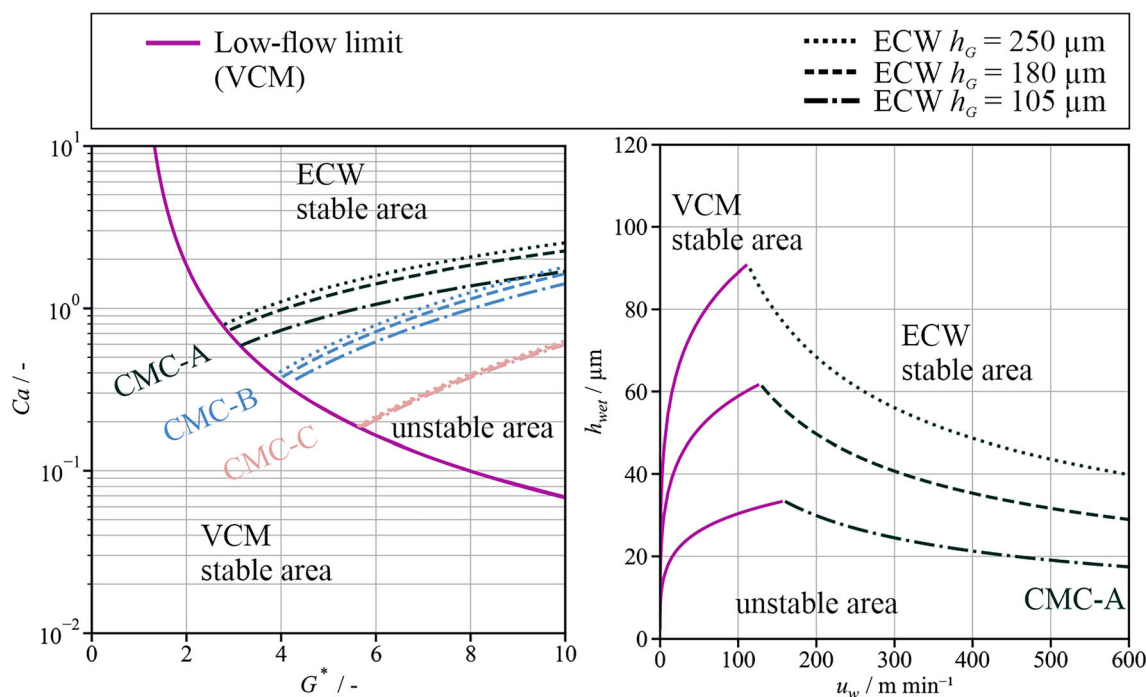


Fig. 7: Calculation of the dimensionless coating window (left) and the dimensional coating window (right) combined from the low-flow limit (VCM) (purple line) and the extended coating window (ECW) (intermittent lines) for the investigated coating gaps ($h_G = 250 \mu\text{m}$ dotted line, $h_G = 180 \mu\text{m}$ dashed line, $h_G = 105 \mu\text{m}$ dash-dot line) for each material system (CMC-A dark green, CMC-B medium blue, CMC-C light red)

due to inertia effects at higher coating speeds, the minimum wet film thickness passes through a maximum and follows the decreasing trend of the extended coating window. For both limits, decreasing the coating gap decreases the minimum wet film thickness.

Validation of the model

To show the accuracy of the calculation, experimental critical length of the boundary layer $L_{b,exp}^*$ and calculated critical length of the boundary layer $L_{b,calc}^*$ of all model systems and coating gap settings are plotted in Fig. 8.

The overall accuracy of $L_{b,calc}^*$ compared with $L_{b,exp}^*$ is sufficiently good. Deviations can be justified by errors in the experimental data (e.g., setting of the coating gap). The errors due to the maximum possible deviation of the set coating gap of $\Delta h_G = \pm 10 \mu\text{m}$ are taken into account in the calculations of the low-flow-limit and the extended coating window and are represented by a shaded area around the calculated lines in the following graphs.

Influence of coating gap on process stability

In Fig. 9, the prediction of the coating window and the experimental data for material system CMC-A (highest viscosity) are shown for different coating gap settings in dimensionless (left) and dimensional form (right).

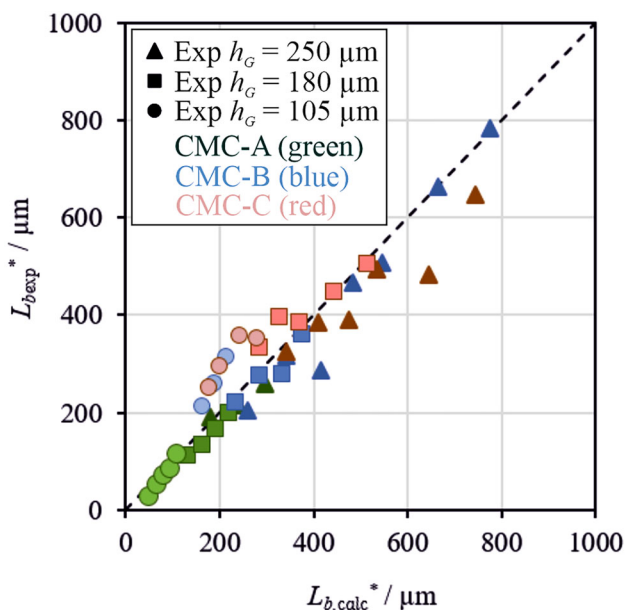


Fig. 8: Experimental critical length of the boundary layer $L_{b,exp}^*$ as a function of calculated critical length of the boundary layer $L_{b,calc}^*$

In both representations of the coating window, the experimental data and the calculations including the deviation of the coating gap setting of $\Delta h_G = \pm 10 \mu\text{m}$ show good agreement. Some of the experimental values are slightly below or above the calculation, but clearly follow the low-flow limit model.

In case of the dimensionless coating window (Fig. 9, left), the critical capillary number of the dimensionless low-flow limit increases with decreasing dimensionless coating gap for each coating gap. The dimensionless coating gaps reach a minimum in the dimensionless coating window and follow the calculation of the extended coating window after the individual transition point (intersections of the purple line with the interrupted dark green lines). As explained in Fig. 7, an increasing coating gap results in higher capillary numbers and higher dimensionless coating gaps.

In the case of the dimensional coating window (Fig. 9, right), the minimum wet film thickness increases with increasing coating speed due to the low-flow limit. For a coating gap of $250 \mu\text{m}$, the experimental values of the minimum wet film thickness increase in agreement with the calculation with the coating speed until 100 m min^{-1} to $98 \mu\text{m}$, for a coating gap of $180 \mu\text{m}$ until 70 m min^{-1} to $53 \mu\text{m}$, and for a coating gap of $105 \mu\text{m}$ until 100 m min^{-1} to $30 \mu\text{m}$. After reaching the described maximum of the low-flow limit, there is a transition point where the experimental values of the minimum wet film thickness decrease with increasing coating speed and follow the calculation of the extended coating window (intersections of the purple line with the interrupted dark green lines). For a coating gap of $250 \mu\text{m}$, the experimental values of the wet film thickness decrease to $67 \mu\text{m}$ at 200 m min^{-1} , for a coating gap of $180 \mu\text{m}$ to $38 \mu\text{m}$ at 300 m min^{-1} and for a coating gap of $105 \mu\text{m}$ to $20 \mu\text{m}$ at 500 m min^{-1} . For coating gap settings of $250 \mu\text{m}$ and $180 \mu\text{m}$, the experimental values of the minimum wet film thickness would theoretically continue to decrease with increasing coating speed, but with the high viscosity of material system CMC-A it was impossible to experimentally determine stable values of wet film thickness at coating speeds above 200 and 300 m min^{-1} , respectively. The volume flow in the experimental setup was limited due to the high pressure drop resulting from high viscosity at high coating speeds.

Nevertheless, the experimental data for material system CMC-A show that the coating gap can be reduced to achieve the required low wet film thicknesses for primer coatings as adhesive layers. In this case, wet film thicknesses of $20\text{--}25 \mu\text{m}$ can be achieved with a coating gap of $105 \mu\text{m}$ at a coating speed of 500 m min^{-1} .

In Fig. 10, the calculated coating windows and the experimental data for material system CMC-C (lowest viscosity) are shown for different coating gaps. In Fig. 10 (left), the dimensionless coating window and in Fig. 10 (right) the dimensional coating window is shown.

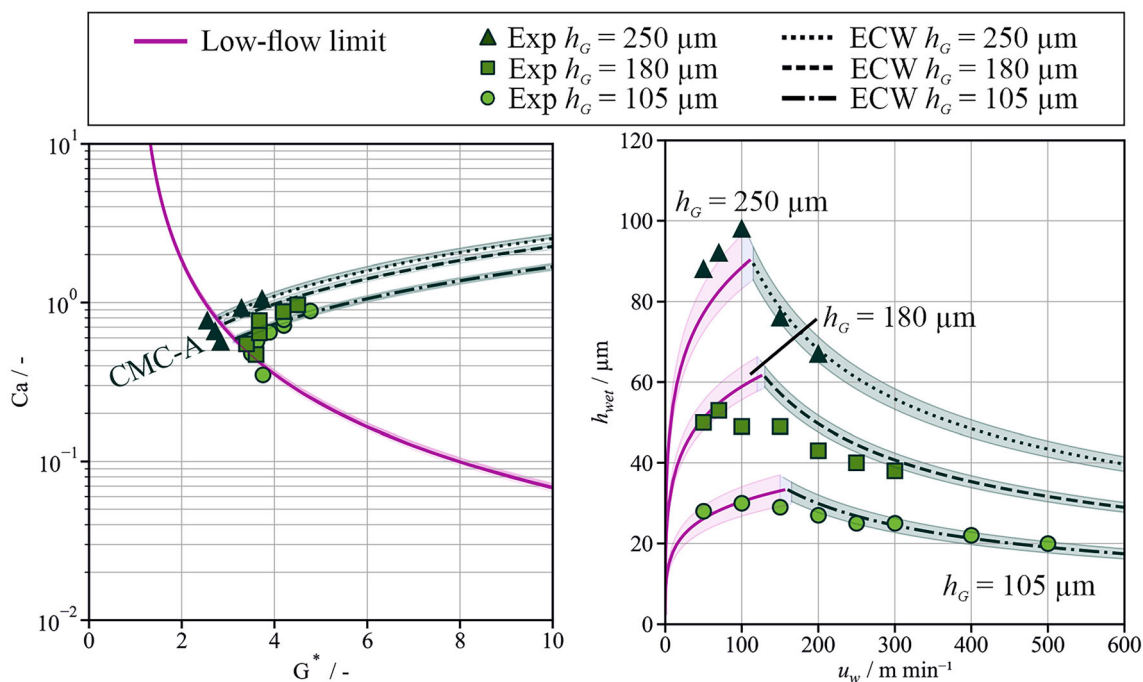


Fig. 9: Calculation and experimental data of the dimensionless coating window (left) and the dimensional coating window (right) combined from the low-flow limit (VCM) (purple line) and the extended coating window (ECW) (intermittent lines) for the investigated coating gaps ($h_G = 250 \mu\text{m}$ dotted line, $h_G = 180 \mu\text{m}$ dashed line, $h_G = 105 \mu\text{m}$ dash-dot line) and experimental data ($h_G = 250 \mu\text{m}$ triangle, $h_G = 180 \mu\text{m}$ square, $h_G = 105 \mu\text{m}$ circle) for material system CMC-A. The colored shadows around the calculated lines represent the deviation of the calculations of the low-flow-limit (purple) and the extended coating window (dark green) due to the maximum possible deviation of the set coating gap of $\Delta h_G = \pm 10 \mu\text{m}$

The experimental data and the calculations of the low-flow limit including the deviation of the coating gap setting of $\Delta h_G = \pm 10 \mu\text{m}$ show good agreement in both representations of the coating window. In case of the dimensionless coating window (Fig. 10, left), the critical capillary number of the low-flow limit increases with decreasing dimensionless coating gap for all investigated coating gaps. As previously explained, the dimensionless coating gaps reach a minimum in the dimensionless coating window and follow the calculation of the extended coating window after individual transition points (intersections of the purple line with the interrupted light red lines). Increasing coating gaps lead to higher capillary numbers and higher dimensionless coating gaps. As explained in Fig. 7, a decreasing viscosity leads to a decreasing influence of the coating gap on the coating window. In the case of a coating gap of $105 \mu\text{m}$, the experimental values of the capillary number and the dimensionless coating gap deviate from the calculated low-flow limit and the extended coating window including the deviation from the coating gap setting. For very small coating gaps, the VCM may no longer be valid due to the high viscous pressure drop. The neglect of the pressure drop in the coating gap in the calculation of the extended coating window could cause the calculation to deviate from the experimental data.

In the case of the dimensional coating window (Fig. 10, right), the minimum wet film thickness increases with increasing coating speed for the low-flow-limit. For the coating gap of $250 \mu\text{m}$, the experimental values of the minimum wet film thickness increase to $42 \mu\text{m}$ at a coating speed of 150 m min^{-1} , for a coating gap of $180 \mu\text{m}$ to $34 \mu\text{m}$ at 150 m min^{-1} , and for a coating gap of $105 \mu\text{m}$ to $24 \mu\text{m}$ at 250 m min^{-1} . After reaching the described maximum of the low-flow limit, the experimental values of the minimum wet film thickness reach the individual transition point and decrease with increasing coating speed, following the calculation of the extended coating window (intersections of the purple line with the interrupted light red lines). For a coating gap of $250 \mu\text{m}$, the experimental values of the wet film thickness decrease to $27 \mu\text{m}$, for a coating gap of $180 \mu\text{m}$ to $23 \mu\text{m}$ and for a coating gap of $105 \mu\text{m}$ to $18 \mu\text{m}$ at a coating speed of 500 m min^{-1} . In the case of a coating gap of $105 \mu\text{m}$, the experimental values of the minimum wet film thickness of the extended coating window exceed the calculated ones, including the deviation from the coating gap setting on average by 19.0 % and $3.4 \mu\text{m}$. For material system CMC-C, the required wet film thicknesses of typical primer coatings for adhesive layers of approx. $20\text{--}25 \mu\text{m}$ can be achieved with a coating gap of $180 \mu\text{m}$ at a coating speed of 500 m min^{-1} .

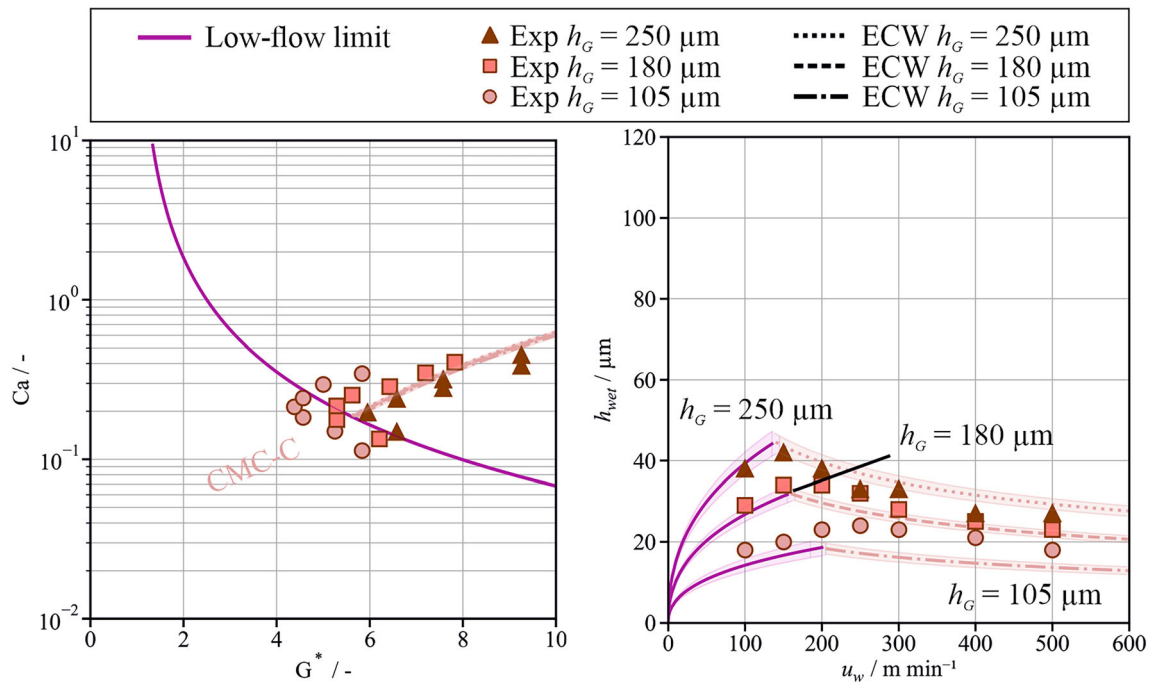


Fig. 10: Calculation of the dimensionless coating window (left) and the dimensional coating window (right) combined from the low-flow limit (VCM) (purple line) and the extended coating window (ECW) (intermittent lines) for the investigated coating gaps ($h_G = 250 \mu\text{m}$ dotted line, $h_G = 180 \mu\text{m}$ dashed line, $h_G = 105 \mu\text{m}$ dash-dot line) and experimental data ($h_G = 250 \mu\text{m}$ triangle, $h_G = 180 \mu\text{m}$ square, $h_G = 105 \mu\text{m}$ circle) for material system CMC-C (light red). The colored shadows around the calculated lines represent the deviation of the calculations of the low-flow-limit (purple) and the extended coating window (light red) due to the maximum possible deviation of the set coating gap of $\Delta h_G = \pm 10 \mu\text{m}$

The calculations of the dimensionless and dimensional coating window combined from the low-flow limit and the extended coating window for material system CMC-B (medium blue) are shown in the supporting information. The experimental data of material system CMC-B also follow the prediction model of the coating window.

Influence of viscosity on process stability

In Fig. 11, the predicted coating windows and the experimental data for all investigated material systems (CMC-A, CMC-B and CMC-C) are shown for a constant coating gap of 250 μm . In Fig. 11 (left), the dimensionless coating window, and in Fig. 11 (right), the dimensional coating window, are shown.

Comparing the experimental data and the prediction model for the different material systems at a constant coating gap of 250 μm , for both representations of the coating window there is a good agreement. For all model systems, the critical capillary number of the low-flow limit increases with decreasing dimensionless coating gap (Fig. 11, left). As described earlier, the dimensionless coating gaps reach a minimum in the dimensionless coating window and follow the calculation of the extended coating window (intersections of the purple line with the interrupted dark green, medium blue and light red lines). Decreasing viscosity

leads to lower capillary numbers and lower dimensionless coating gaps.

In the case of the dimensional coating window (Fig. 11, right) and as previously discussed, the minimum wet film thickness of all material systems increases with increasing coating speed for the low-flow-limit. For material system CMC-A, the experimental values of the minimum wet film thickness increase until a coating speed of 100 m min^{-1} to 98 μm , and for material system CMC-B until 100 m min^{-1} to 62 μm , and for material system CMC-C until 150 m min^{-1} to 42 μm . After reaching the individual transition point, the minimum wet film thicknesses decrease with increasing coating speed with the prediction of the extended coating window (intersections of the purple line with the interrupted dark green, medium blue and light red lines). For material system CMC-A, the experimental values of the wet film thickness decrease to 67 μm at 200 m min^{-1} , for material system CMC-B to 42 μm at 400 m min^{-1} and for material system CMC-C to 27 μm at 500 m min^{-1} . For material systems CMC-A and CMC-B it was impossible to stabilize the coating at higher coating speeds. As explained earlier, the volume flow was limited due to increasing pressure drop with increasing viscosity.

The comparison of the dimensionless and dimensional coating window combined from the low-flow limit and the extended coating window for all material

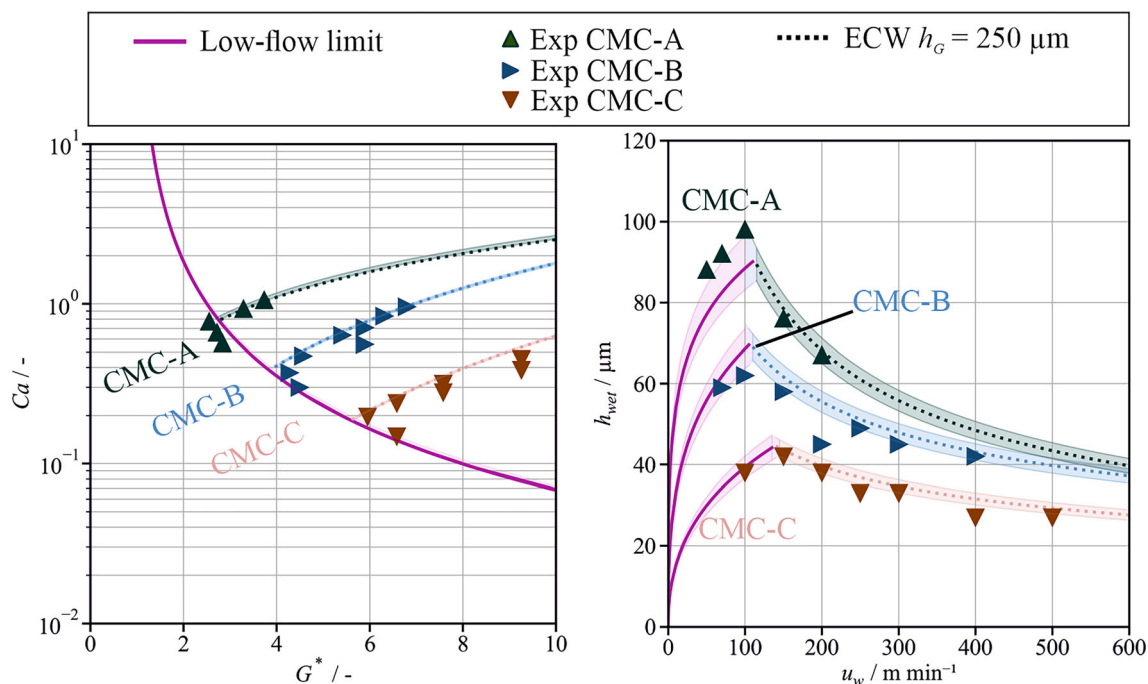


Fig. 11: Calculation of the dimensionless coating window (left) and the dimensional coating window (right) combined from the low-flow limit (VCM) (purple line) and the extended coating window (ECW) (intermittent lines) for each material system (CMC-A dark green, CMC-B medium blue, CMC-C light red) and experimental data (CMC-A dark green triangle down, CMC-B medium blue triangle right, CMC-C light red triangle) for the investigated coating gap $h_G = 250 \mu\text{m}$ (dotted line). The colored shadows around the calculated lines represent the deviation of the calculations of the low-flow-limit (purple) and the extended coating window (CMC-A dark green, CMC-B medium blue, CMC-C light red) due to the maximum possible deviation of the set coating gap of $\Delta h_G = \pm 10 \mu\text{m}$

systems for the other coating gap settings $105 \mu\text{m}$ and $180 \mu\text{m}$ is shown in the supporting information.

Conclusions

In order to cover a wide range of use cases of thin films, the influence of coating gap and viscosity of shear-thinning fluids on the coating window of high-speed coating with slot die and vacuum box was investigated. In addition, with the gained knowledge, a prediction model combining the low-flow limit and the extended coating window was developed. It was shown that the prediction of the coating window with the combined model is possible for the investigated material systems and coating gaps over the investigated range of coating speeds (until 500 m min^{-1}). Decreasing viscosity leads to smaller values of the minimum wet film thickness, larger dimensionless coating gaps and smaller capillary numbers. In addition, a decreasing coating gap leads to smaller values of the minimum wet film thickness, larger dimensionless coating gaps and smaller capillary numbers. Consequently, the coating gap must be adjusted to achieve the target wet film thickness and, therefore, the target layer thickness for different material properties used for different coating applications. For the most viscous material system CMC-A, it

is possible to reach typical wet film thicknesses of primer coatings for adhesive layers of $20\text{--}25 \mu\text{m}$ with a coating gap of $105 \mu\text{m}$ at a coating speed of 500 m min^{-1} . The same target wet film thickness was reached for material system CMC-C with 2.5 times lower viscosity comparing the corresponding shear rates with a coating gap of $180 \mu\text{m}$ at a coating speed of 500 m min^{-1} .

Acknowledgments The authors would like to acknowledge financial support of the Federal Ministry of Education and Research (BMBF) via the ProZell cluster-project ‘‘HiStructures’’ (Grant No.: 03XP0243C) and the Deutsche Forschungsgemeinschaft (DFG, German Research Foundation) under Germany’s Excellence Strategy – EXC 2154 – Project number 390874152 (POLiS Cluster of Excellence). This work contributes to the research conducted at the Center for Electrochemical Energy Storage Ulm-Karlsruhe (CELEST) and Material Research Center for Energy Systems (MZE).

Funding Open Access funding enabled and organized by Projekt DEAL.

Conflict of interest The authors declare no conflict of interest.

Open Access This article is licensed under a Creative Commons Attribution 4.0 International License, which permits use, sharing, adaptation, distribution and reproduction in any medium or format, as long as you give appropriate credit to the original author(s) and the source, provide a link to the Creative Commons licence, and indicate if changes were made. The images or other third party material in this article are included in the article's Creative Commons licence, unless indicated otherwise in a credit line to the material. If material is not included in the article's Creative Commons licence and your intended use is not permitted by statutory regulation or exceeds the permitted use, you will need to obtain permission directly from the copyright holder. To view a copy of this licence, visit <http://creativecommons.org/licenses/by/4.0/>.

References

- Jaiser, S, Müller, M, Baunach, M, Bauer, W, Scharfer, P, Schabel, W, "Investigation of film solidification and binder migration during drying of Li-ion battery anodes." *J. Power Sour.*, **318** 210–219 (2016)
- Kumberg, J, Müller, M, Diehm, R, Spiegel, S, Wachsmann, C, Bauer, W, Scharfer, P, Schabel, W, "Drying of lithium-ion battery anodes for use in high-energy cells: influence of electrode thickness on drying time, adhesion, and crack formation." *Energy Technol.*, **7** (11) 1900722 (2019)
- Lim, S, Ahn, KH, Yamamura, M, "Latex migration in battery slurries during drying." *Langmuir*, **29** (26) 8233–8244 (2013)
- Doberdò, I, Löffler, N, Laszczynski, N, Cericola, D, Penazzi, N, Bodoardo, S, Kim, G-T, Passerini, S, "Enabling aqueous binders for lithium battery cathodes – Carbon coating of aluminum current collector." *J. Power Sour.*, **248** 1000–1006 (2014)
- Li, C-C, Lee, J-T, Tung, Y-L, Yang, C-R, "Effects of pH on the dispersion and cell performance of LiCoO₂ cathodes based on the aqueous process." *J. Mater. Sci.*, **42** (14) 5773–5777 (2007)
- Kimura, K, Sakamoto, T, Mukai, T, Ikeuchi, Y, Yamashita, N, Onishi, K, Asami, K, Yanagida, M, "Improvement of the cyclability and coulombic efficiency of Li-ion batteries using Li[Ni_{0.8}Co_{0.15}Al_{0.05}]O₂ cathode containing an aqueous binder with pressurized CO₂ gas treatment." *J. Electrochem. Soc.*, **165** (2) A16–A20 (2018)
- Bockholt, H, Indrikova, M, Netz, A, Golks, F, Kwade, A, "The interaction of consecutive process steps in the manufacturing of lithium-ion battery electrodes with regard to structural and electrochemical properties." *J. Power Sour.*, **325** 140–151 (2016)
- Kremer, LS, Hoffmann, A, Danner, T, Hein, S, Prifling, B, Westhoff, D, Dreer, C, Latz, A, Schmidt, V, Wohlfahrt-Mehrens, M, "Manufacturing process for improved ultrathick cathodes in high-energy lithium-ion batteries." *Energy Technol.*, **8** (2) 1900167 (2020)
- Hoffmann, A, Heider, EA, Dreer, C, Pfeifer, C, Wohlfahrt-Mehrens, M, "Influence of the mixing and dispersing process on the slurry properties and the microstructure and performance of ultrathick cathodes for lithium-ion batteries." *Energy Technol.*, **11** (5) 2200484 (2022)
- Kumberg, J, Bauer, W, Schmatz, J, Diehm, R, Tönsmann, M, Müller, M, Ly, K, Scharfer, P, Schabel, W, "Reduced drying time of anodes for lithium-ion batteries through simultaneous multilayer coating." *Energy Technol.*, **9** (10) 2100367 (2021)
- Singh, M, Kaiser, J, "Thick electrodes for high energy." *J. Electrochem. Soc.*, **162** (7) A1196 (2015)
- Singh, M, Kaiser, J, Hahn, H, "A systematic study of thick electrodes for high energy lithium ion batteries." *J. Electroanal. Chem.*, **782** 245–249 (2016)
- Klemens, J, Schneider, L, Herbst, EC, Bohn, N, Müller, M, Bauer, W, Scharfer, P, Schabel, W, "Drying of NCM cathode electrodes with porous, nanostructured particles versus compact solid particles: comparative study of binder migration as a function of drying conditions." *Energy Technol.*, **10** (4) 2100985 (2022)
- Klemens, J, Burger, D, Schneider, L, Spiegel, S, Müller, M, Bohn, N, Bauer, W, Ehrenberg, H, Scharfer, P, Schabel, W, "Drying of compact and porous NCM cathode electrodes in different multilayer architectures: influence of layer configuration and drying rate on electrode properties." *Energy Technol.*, **1** (8) 2300267 (2023)
- Chen, L-C, Liu, D, Liu, T-J, Tiu, C, Yang, C-R, Chu, W-B, Wan, C-C, "Improvement of lithium-ion battery performance using a two-layered cathode by simultaneous slot-die coating." *J. Energy Storage*, **5** 156–162 (2016)
- Müller, M, Pfaffmann, L, Jaiser, S, Baunach, M, Trouillet, V, Scheiba, F, Scharfer, P, Schabel, W, Bauer, W, "Investigation of binder distribution in graphite anodes for lithium-ion batteries." *J. Power Sour.*, **340** 1–5 (2017)
- Diehm, R, Kumberg, J, Dörrer, C, Müller, M, Bauer, W, Scharfer, P, Schabel, W, "In situ investigations of simultaneous two-layer slot die coating of component-graded anodes for improved high-energy Li-ion batteries." *Energy Technol.*, **8** (5) 1901251 (2020)
- Schmitt, M, Raupp, S, Wagner, D, Scharfer, P, Schabel, W, "Analytical determination of process windows for bilayer slot die coating." *J. Coat. Technol. Res.*, **12** (5) 877–887 (2015)
- Liu, D, Chen, L-C, Liu, T-J, Chu, W-B, Tiu, C, "Improvement of lithium-ion battery performance by two-layered slot-die coating operation." *Energy Technol.*, **5** (8) 1235–1241 (2017)
- Gottschalk, L, Oertel, C, Strzelczyk, N, Müller, J, Krüger, J, Haselrieder, W, Kwade, A, "Improving the performance of lithium-ion batteries using a two-layer, hard carbon-containing silicon anode for use in high-energy electrodes." *Energy Technol.*, **11** (5) 2200858 (2022)
- Diehm, R, Müller, M, Burger, D, Kumberg, J, Spiegel, S, Bauer, W, Scharfer, P, Schabel, W, "High-speed coating of primer layer for Li-ion battery electrodes by using slot-die coating." *Energy Technol.*, **8** (9) 2000259 (2020)
- Li, T, "Carbon-coated aluminum foil as current collector for improving the performance of lithium sulfur batteries." *Int. J. Electrochem. Sci.*, **12** (4) 3099–3108 (2017)
- Lee, S, Oh, E-S, "Performance enhancement of a lithium ion battery by incorporation of a graphene/polyvinylidene fluoride conductive adhesive layer between the current collector and the active material layer." *J. Power Sour.*, **244** 721–725 (2013)
- Busson, C, Blin, M-A, Guichard, P, Soudan, P, Crosnier, O, Guyomard, D, Lestriez, B, "A primed current collector for high performance carbon-coated LiFePO₄ electrodes with no carbon additive." *J. Power Sour.*, **406** 7–17 (2018)
- Wood, DL, Quass, JD, Li, J, Ahmed, S, Ventola, D, Daniel, C, "Technical and economic analysis of solvent-based

- lithium-ion electrode drying with water and NMP.” *Drying Technology*, **36** (2) 234–244 (2018)
26. Carvalho, MS, Khesghi, HS, “Low-flow limit in slot coating: Theory and experiments.” *AIChE J*, **46** (10) 1907–1917 (2000)
 27. Kistler, SF, Schweizer, PM, *Liquid Film Coating. Scientific Principles and Their Technological Implications*. Springer, Netherlands, Dordrecht (2012)
 28. Romero, OJ, Suszynski, WJ, Scriven, LE, Carvalho, MS, “Low-flow limit in slot coating of dilute solutions of high molecular weight polymer.” *J. Non-Newton. Fluid Mech.*, **118** (2–3) 137–156 (2004)
 29. Ruschak, KJ, “Limiting flow in a pre-metered coating device.” *Chem. Eng. Sci.*, **31** (11) 1057–1060 (1976)
 30. Schmitt, M, Baunach, M, Wengeler, L, Peters, K, Junges, P, Scharfer, P, Schabel, W, “Slot-die processing of lithium-ion battery electrodes—Coating window characterization.” *Chem. Eng. Process. Process Intensif.*, **68** 32–37 (2013)
 31. Landau, LD, Levich, BC, “Dragging of a liquid by a moving plate.” *Acta Physicochim.*, **17** 42–54 (1942)
 32. Schmitt, M, *Slot Die Coating of Lithium-Ion Battery Electrodes* (2016)
 33. Sakiadis, BC, “Boundary-layer behavior on continuous solid surfaces: II. The boundary layer on a continuous flat surface.” *AIChE J*, **7** (2) 221–225 (1961)
 34. Hens, J, Boiy, L, “Operation of the bead of a pre-metered coating device.” *Chem. Eng. Sci.*, **41** (7) 1827–1831 (1986)
 35. Arzate, A, Tanguy, PA, “Hydrodynamics of liquid jet application in high-speed jet coating.” *Chem. Eng. Res. Des.*, **83** (2) 111–125 (2005)

Publisher’s Note Springer Nature remains neutral with regard to jurisdictional claims in published maps and institutional affiliations.